
Article:
Karadakov, Peter Borislavov orcid.org/0000-0002-2673-6804, Stewart, Ben and Cooper, David L. (2023) Magnetic Shielding Analysis of Bonding in [1.1.1]Propellane. Journal of Physical Chemistry A. pp. 861-869. ISSN 1089-5639

https://doi.org/10.1021/acs.jpca.2c06450

THE JOURNAL OF PHYSICAL CHEMISTRY A
A JOURNAL OF THE AMERICAN CHEMICAL SOCIETY

pubs.acs.org/JPCA

Article

Magnetic Shielding Analysis of Bonding in [1.1.1]Propellane

Peter B. Karadakov,* Ben Stewart, and David L. Cooper

Cite This: https://doi.org/10.1021/acs.jpca.2c06450

Read Online

ACCESS | Metrics & More | Article Recommendations | Supporting Information

ABSTRACT: The bonding in [1.1.1]propellane, bicyclo[1.1.0]-butane, bicyclo[1.1.1]pentane, tetrahedrane, and cyclopropane is investigated by analyzing changes in the off-nucleus isotropic magnetic shielding within the space surrounding each of these molecules and, for [1.1.1]propellane, by examining also the diamagnetic and paramagnetic contributions to this shielding. Any shielding arising from the two "exo" sp^3-like hybrid atomic orbitals on the bridgehead carbon atoms that have been used to support the idea of an inverted bond between these two atoms is found to be almost entirely contained within the [1.1.1]propellane cage and to contribute to a strongly shielded central region. This strongly shielded region suggests the establishment of a mainly covalent bonding interaction involving all carbon atoms that cannot be straightforwardly decomposed into contributions from individual carbon−carbon bonds. The emergence of the strongly shielding central region is traced by comparing the shielding variations in and around molecules with one three-membered carbon ring (cyclopropane), two fused three-membered carbon rings (bicyclo[1.1.0]butane), and three fused three-membered carbon rings ([1.1.1]propellane).

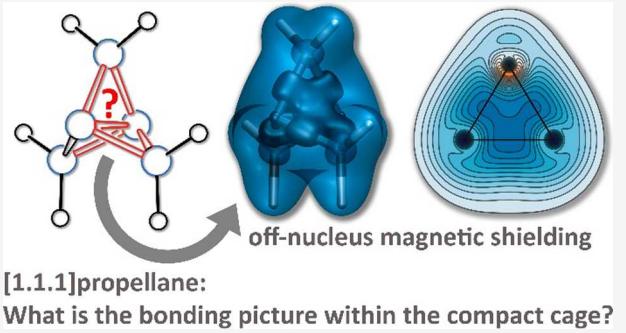

INTRODUCTION

Bonding in [1.1.1]propellane (tricyclo[1.1.1.$0^{1,3}$]pentane) and, in particular, the questions of whether there is a central bond connecting the two bridgehead carbon atoms and, if so, what is the nature of that bond, have been debated by theoretical chemists over many years.[1] If it is present, a bond between the bridgehead carbon atoms would imply that [1.1.1]propellane incorporates three three-membered carbon rings fused along that bond. The prevalent view in the literature, mostly based on breathing-orbital valence bond (BOVB) calculations,[2] is that this central bond does exist and that it is an example of a so-called charge-shift bond (CSB).[3] In the BOVB description, the bond between the bridgehead carbon atoms is established with the participation of two "exo" sp^3-like hybrid atomic orbitals (HAOs) pointing outward of the [1.1.1]propellane cage and, as a consequence, the bond is said to be "inverted." In contrast to standard covalent bonds, its strength arises in BOVB calculations from resonance between covalent and ionic components, C··C ↔ (C^+:C^- + C^-:C^+). The covalent component C··C, which involves the singlet-coupled electrons in the two HAOs, is thought not to be sufficiently "bonding" to overcome the large repulsions from the six "wing" C−C bonds, and hence the need to bring in the ionic components, which are also insufficient on their own to explain the bonding. Such views, and indeed the very existence of the inverted bond, are still actively being queried[4] and defended robustly.[5] Certainly, it has been shown that localization of the two active space orbitals in a CASSCF(2,2) wavefunction (complete active space self-consistent field with "2 electrons in 2 orbitals") for [1.1.1]propellane leads to a description of the inverted bond that resembles closely the CSB model;[6] one difference from the BOVB wavefunction is that the localized CASSCF(2,2) active space orbitals are orthogonal, which "pushes" them further out of the interior of the cage. Even so, this does mean that a wavefunction incorporating the essential features of the CSB model for the inverted bond in [1.1.1]propellane had been used to describe this molecule many years ago because the two-configuration SCF (TCSCF) wavefunction that was employed by Feller and Davidson[7] is equivalent to a CASSCF(2,2) construction.

In this paper, we present a different interpretation of the bonding in [1.1.1]propellane. Instead of looking for individual carbon−carbon bonds and then trying to elucidate their nature and interactions, we analyze the overall bonding picture within the [1.1.1]propellane cage using a visual approach that involves the calculation of the off-nucleus isotropic magnetic shielding, $\sigma_{iso}(\mathbf{r})$, as a function of position in the space surrounding the molecule. The most popular example of an off-nucleus shielding in chemistry is the nucleus-independent chemical shift (NICS),[8] an aromaticity criterion suggested by Schleyer and co-workers which, in its original definition, uses a single

Received: September 9, 2022
Revised: December 17, 2022

isotropic shielding calculated at the center of an aromatic or antiaromatic ring and taken with an inversed sign.[9] The approach we use is closer in spirit to the work of Wolinski[10] who analyzed the changes in the off-nucleus shielding tensor along the molecular axes of linear molecules and to the isotropic shielding isosurfaces investigated by Klod and Kleinpeter.[11] An off-nucleus magnetic shielding tensor $\boldsymbol{\sigma}(\mathbf{r})$ can be calculated, in analogy to the nuclear magnetic shielding tensor, as a second-order response property.[10]

$$\sigma_{\alpha\beta}(\mathbf{r}) = \left.\frac{\partial^2 E(\mathbf{B}, \{\mathbf{m}\})}{\partial m_\alpha(\mathbf{r}) \partial B_\beta}\right|_{\mathbf{B}=\mathbf{0},\forall\,\mathbf{m}=\mathbf{0}} \quad (1)$$

where $E(\mathbf{B}, \{\mathbf{m}\})$ is the energy of the molecule in the presence of an external magnetic field $\mathbf{B}$, $\{\mathbf{m}\}$ stands for the collection of magnetic moments of the nuclei and of suitable probes, say, neutrons,[10] placed at $\mathbf{r}$ and at any other off-nucleus locations of interest, and α and β denote the Cartesian coordinates x, y, and z. Differentiating $E(\mathbf{B}, \{\mathbf{m}\})$ with respect to $m_\alpha(\mathbf{r})$ first leads to the expression[12,13]

$$\sigma_{\alpha\beta}(\mathbf{r}) = \sum_{p,q}\left[D_{pq}(\mathbf{B}, \{\mathbf{m}\})\frac{\partial^2 h_{qp}(\mathbf{B}, \{\mathbf{m}\})}{\partial m_\alpha(\mathbf{r}) \partial B_\beta}\right]_{\mathbf{B}=\mathbf{0},\forall\,\mathbf{m}=\mathbf{0}} + \sum_{p,q}\left[\frac{\partial D_{pq}(\mathbf{B}, \{\mathbf{m}\})}{\partial B_\beta}\frac{\partial h_{qp}(\mathbf{B}, \{\mathbf{m}\})}{\partial m_\alpha(\mathbf{r})}\right]_{\mathbf{B}=\mathbf{0},\forall\,\mathbf{m}=\mathbf{0}} \quad (2)$$

where $D_{pq}(\mathbf{B}, \{\mathbf{m}\})$ and $h_{qp}(\mathbf{B}, \{\mathbf{m}\})$ are elements of the one-electron density matrix and of the one-electron part of the Hamiltonian, respectively, in terms of gauge-including atomic orbitals (GIAOs). The off-nucleus isotropic magnetic shielding corresponding to eq 2 is defined as $\sigma_{iso}(\mathbf{r}) = 1/3[\sigma_{xx}(\mathbf{r}) + \sigma_{yy}(\mathbf{r}) + \sigma_{zz}(\mathbf{r})]$. The two terms in eq 2 can be assumed to correspond to the diamagnetic and paramagnetic contributions to the shielding tensor, $\boldsymbol{\sigma}(\mathbf{r}) = \boldsymbol{\sigma}^{d}(\mathbf{r}) + \boldsymbol{\sigma}^{p}(\mathbf{r})$; if use is made of the natural orbital connection,[14−16] this assumption has been shown to work well for nuclear shieldings[16] and it can be shown to work equally well for off-nucleus shieldings. The natural orbital connection ensures maximum similarity, in a least-squares sense, between the orthonormalized perturbed molecular orbitals (MOs) and the unperturbed (unmodified) MOs.[17] This connection provides a suitable partitioning of the shielding tensors defined in terms of GIAOs into diamagnetic and paramagnetic contributions which coincide in the basis set limit with the usual definitions for perturbation-independent AOs.

According to eq 2, the diamagnetic contribution depends on the one-electron density matrix, and the paramagnetic contribution depends on the extent to which the elements of this density matrix can be perturbed by an external magnetic field. We note that the derivatives $\partial D_{pq}(\mathbf{B}, \{\mathbf{m}\})/\partial B_\beta$ are imaginary and, therefore, to first order, the one-electron density matrix does not change as a result of the perturbation. The electron density along a chemical bond, when exposed to an external magnetic field, shields the bond and this shielding persists even if the strength of the magnetic field approaches zero. The shielding along and around a bond can be examined by calculating off-nucleus shieldings and their diamagnetic and paramagnetic contributions at a number of points within the space surrounding the bond; the data at these points can be assembled into an isosurface or a contour plot. The balance between the two terms in eq 2 is such that the off-nucleus isotropic magnetic shielding usually increases and reaches a maximum near the midpoint of a bond, rendering most of the bond well-shielded, in contrast to electron density which quickly decreases away from atoms. Hence, off-nucleus isotropic shielding plots usually show higher levels of bond-specific details over the whole length of a chemical bond, which makes the differences between bonds easy to visualize.[18] As a rule, the shielding over a bond increases with bond multiplicity and, in most cases, stronger bonds are more shielded than weaker bonds. For example, analysis of the changes in $\sigma_{iso}(\mathbf{r})$ has been used to demonstrate that the carbon−carbon bond in dicarbon, C_2, is "bulkier," which is consistent with higher multiplicity, but also weaker than the triple carbon−carbon bond in ethyne, C_2H_2.[19] It is interesting in this context to note that C_2 was of direct relevance to an earlier description of the bonding in [1.1.1]propellane in terms of three-center two-electron "σ-bridged π bonds," arising from the interaction of the MOs on a C_2 moiety and on the three methylene (CH_2) fragments.[20] In conjugated cyclic systems with higher-energy π electrons, such as cyclobutadiene, the balance between the two terms in eq 2 can change in favor of the negative second term above and below the ring, leading to the appearance of a distinctly deshielded dumbbell-shaped region which decreases shielding over bonds and can be associated with antiaromaticity.[21,22] On the other hand, strongly shielded central regions have been observed in shielding calculations on singlet excited states of benzene[22] and cyclooctatetraene.[23]

In order to understand better the bonding pattern established within the very tight space inside the compact propellane cage, we compare the isotropic magnetic shielding distribution around [1.1.1]propellane to those around bicyclo[1.1.1]pentane, in which the hydrogen atoms connected to each bridgehead carbon atom (C_b) prevent the establishment of a C_b−C_b bond, as well as to those around tetrahedrane, the hypothetical hydrocarbon featuring the smallest carbon cage, and around bicyclo[1.1.0]butane and cyclopropane, the smallest examples of molecules with two fused and one three-membered carbon rings, respectively. We also examine the spatial variations around [1.1.1]propellane in the diamagnetic and paramagnetic contributions to shielding, and in the total electron density and its Laplacian.

COMPUTATIONAL DETAILS

The D_{3h} geometries of [1.1.1]propellane and bicyclo[1.1.1]-pentane, the C_{2v} geometry of bicyclo[1.1.0]butane, and the T_d geometry of tetrahedrane were optimized at the B3LYP-D3(BJ)/def2-TZVP level (B3LYP with Grimme's D3 empirical dispersion corrections and Becke−Johnson damping, within the def2-TZVP basis set, as implemented in GAUSSIAN[24]). The D_{3h} geometry of [1.1.1]propellane and the C_{2v} geometry of bicyclo[1.1.0]butane were also optimized at the CASSCF-(2,2)/def2-TZVP level using an active space analogous to that in the TCSCF wavefunction of Feller and Davidson.[7] All optimized geometries were confirmed as local minima through harmonic frequency calculations. For cyclopropane, we used an experimental geometry derived from the analysis of its microwave spectrum.[25]

$\sigma_{iso}(\mathbf{r})$ volume data required for the construction of isosurfaces and contour plots were obtained by means of B3LYP-GIAO/6-311++G(d,p) calculations [B3LYP with gauge-including atomic orbitals, within the 6-311++G(d,p)

https://doi.org/10.1021/acs.jpca.2c06450
J. Phys. Chem. A XXXX, XXX, XXX−XXX

basis set], at the B3LYP-D3(BJ)/def2-TZVP geometries of [1.1.1]propellane, bicyclo[1.1.0]butane, bicyclo[1.1.1]pentane and tetrahedrane, and at the experimental geometry of cyclopropane. Additional $\sigma_{iso}(\mathbf{r})$ volume data were obtained for [1.1.1]propellane and bicyclo[1.1.0]butane by means of CASSCF(2,2)-GIAO/6-311++G(d,p) calculations at the respective CASSCF(2,2)/def2-TZVP geometries. In all volume data calculations, $\sigma_{iso}(\mathbf{r})$ was evaluated on regular three-dimensional grids of points with a spacing of 0.05 Å. To reduce computational effort, shielding tensors were calculated for each grid at the symmetry-unique points (using Abelian symmetry only), and then, data were replicated by symmetry.

For visualization purposes, all $\sigma_{iso}(\mathbf{r})$ values from the B3LYP-GIAO/6-311++G(d,p) calculations on [1.1.1]propellane, bicyclo[1.1.0]butane, bicyclo[1.1.1]pentane, tetrahedrane, and cyclopropane, as well as from the CASSCF(2,2)-GIAO/6-311++G(d,p) calculations on [1.1.1]propellane and bicyclo[1.1.0]butane, were assembled in GAUSSIAN cube files.[26] To enable comparisons of the isotropic nuclear shieldings for the molecules studied in this paper to those for ethane and ethene, B3LYP-GIAO/6-311++G(d,p) calculations for ethane and ethene were carried out at the experimental geometries obtained, respectively, from spectroscopic data[27,28] and from a combination of rotational spectroscopy and quantum chemical calculations.[29]

To construct contour plots for [1.1.1]propellane of the total electron density (ρ) and of the Laplacian of the total electron density ($\nabla^2\rho$), these two quantities were evaluated at the B3LYP/6-311++G(d,p) and CASSCF(2,2)/6-311++G(d,p) levels with the GAUSSIAN CUBEGEN utility program,[26] using two-dimensional grids of points with a spacing of 0.05 Å in one of the σ_v symmetry planes.

All calculations reported in this paper were carried out in the gas phase and were performed using GAUSSIAN,[24] except for the CASSCF(2,2)-GIAO calculations, which were performed using DALTON.[30] All optimized geometries, additional computational details, and the GAUSSIAN cube files with shielding data are included in the Supporting Information.

RESULTS AND DISCUSSION

Key interatomic distances from the geometries of [1.1.1]-propellane **1**, bicyclo[1.1.0]butane **2**, bicyclo[1.1.1]pentane **3**, tetrahedrane **4**, and cyclopropane **5** that were used in the off-nucleus isotropic magnetic shielding calculations are shown in Figure 1.

As is to be expected from previous work,[6] B3LYP underestimates the C_b-C_b distance in **1**, whereas CASSCF-(2,2) gets it about right; a similar situation is observed in **2**. The C_b-C_b distances from our B3LYP-D3(BJ)/def2-TZVP and CASSCF(2,2)/def2-TZVP optimized geometries of **1** are in excellent agreement with those obtained at the B3LYP/def2-QZVPP and CASSCF(2,2)/def2-QZVPP levels, respectively;[6] very close agreement is also observed between the B3LYP-D3(BJ)/def2-TZVP and B3LYP/cc-pVTZ[34] optimized geometries of **3** and its experimental geometry. These observations indicate that the use of larger basis sets and the addition of dispersion corrections to B3LYP have very minor effects on the optimized geometries of **1** and **3**.

The changes in isotropic shielding around **1**−**5** from data computed at the B3LYP level are illustrated in Figure 2. The CASSCF(2,2) isosurfaces for **1** and **2** are visually very similar to the B3LYP ones and so they are not shown here separately (but these isosurfaces can be examined using the corresponding GAUSSIAN cube files in the Supporting Information). We observe that all C−C and C−H bonds in **1**−**5** are well-shielded, in a fashion similar to what has been observed in off-nucleus shielding calculations on other molecules.[18,19] Due to the relatively small separations between the various C−C bonds in **1**−**5**, the shielded regions around these bonds show a tendency to merge together within the $\sigma_{iso}(\mathbf{r})$ = 16 ppm isosurface. There is, however, a "shielding hole" of $\sigma_{iso}(\mathbf{r})$ < 10 ppm near the center of **3** and there are regions of decreased shielding near the centers of **4** and **5**. (These features are easier to observe in the respective contour plots in Figure 3, as discussed later.)

Shielding within the darker regions just outside each of the C−C bonds in cyclopropane **5** exceeds 50 ppm. The positioning of these strongly shielded regions supports the Coulson−Moffitt model of bonding in this molecule,[35] in which three bent C−C bonds are formed from six equivalent HAOs that overlap in pairs just outside the triangle formed by

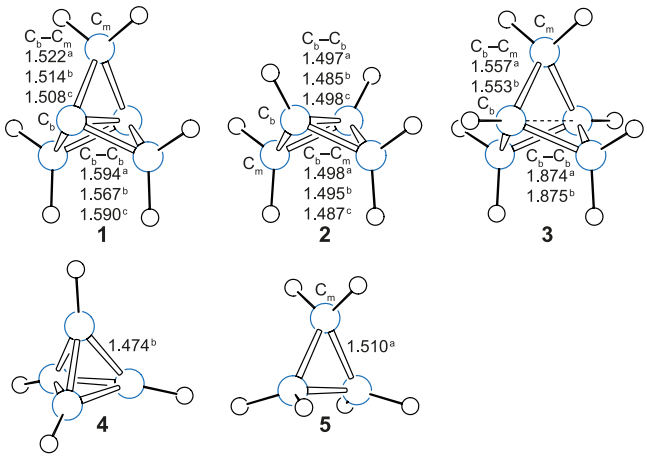

Figure 1. Geometries of [1.1.1]propellane **1**, bicyclo[1.1.0]butane **2**, bicyclo[1.1.1]pentane **3**, tetrahedrane **4**, and cyclopropane **5** with C−C distances (in Å) from [a]experimental geometries (gas-phase electron diffraction for **1**[31] and **3**,[32] microwave spectrum analysis for **2**[33] and **5**[25]), and from [b]B3LYP-D3(BJ)/def2-TZVP and [c]CASSCF(2,2)/def2-TZVP optimized geometries. C_b and C_m in **1**−**3** and **5** denote bridgehead and methylene carbon atoms, respectively.

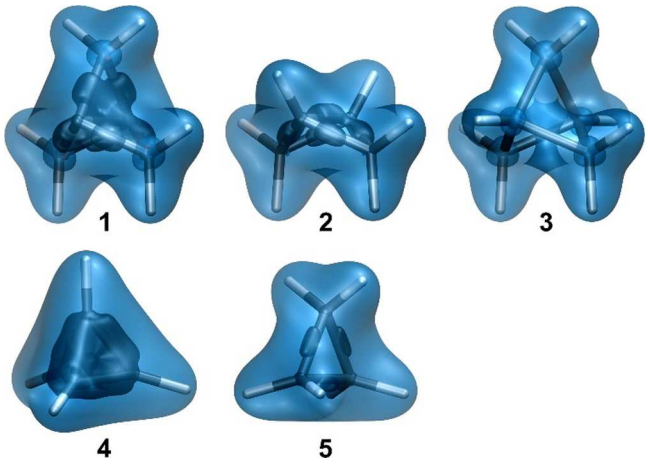

Figure 2. Isotropic shielding isosurfaces for **1**−**5** at $\sigma_{iso}(\mathbf{r}) = \pm 16$ ppm (positive/negative isovalues in blue/orange) and $\sigma_{iso}(\mathbf{r})$ = 50 ppm (darker) [B3LYP-GIAO/6-311++G(d,p)//B3LYP-D3(BJ)/def2-TZVP].

https://doi.org/10.1021/acs.jpca.2c06450
J. Phys. Chem. A XXXX, XXX, XXX−XXX

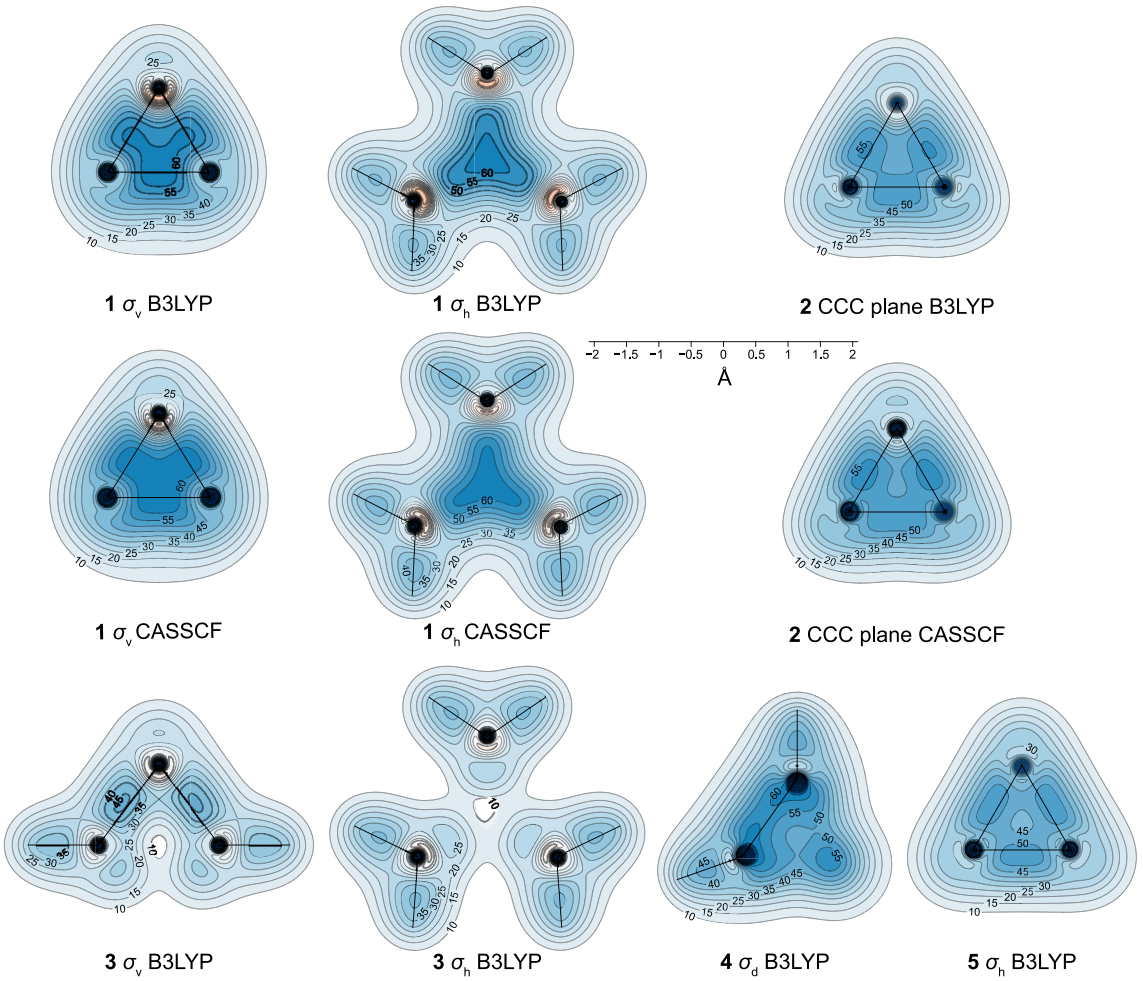

Figure 3. Isotropic shielding contour plots in the σ_v, σ_h, or d σ_d symmetry planes of **1**, **3**−**6** and in one of the CCC planes of **2**, from calculations at the B3LYP-GIAO/6-311++G(d,p)//B3LYP-D3(BJ)/def2-TZVP and CASSCF(2,2)-GIAO/6-311++G(d,p)//CASSCF(2,2)/def2-TZVP levels. Lines show bonds in the plotting plane. $\sigma_{iso}(\mathbf{r})$ range between ca. −20 and 180 ppm, red/orange (deshielded) to blue (shielded).

the three carbon atoms, and is in agreement with the results of spin-coupled generalized VB (SCGVB) calculations.[36] The lower shielding in the ring's interior makes less likely the alternative Walsh model[37] in which the overlap of three carbon sp^2 HAOs pointing toward the center of the ring gives rise to a two-electron three-center bond.

The strongly shielded region encompassing the middle parts of the wing C−C bonds and most of the interior of the [1.1.1]propellane cage in **1** has no counterpart in **3**, where shielding does not reach 50 ppm anywhere in the vicinity of its longer and more widely spaced wing C−C bonds. In contrast to the situation in **5**, we do not observe any signs of repulsive interactions between the wing C−C bonds; in fact, the strongly shielded central region in **1** suggests that most of the shielding over each of these bonds remains inside the cage and contributes to this strongly shielded central region. Connected regions inside which $\sigma_{iso}(\mathbf{r})$ exceeds 50 ppm are also observed in **2** and **4**. While that in **2** is smaller than the corresponding region in **1**, the increased shielding "grips" the wing C−C bonds in a very similar manner. The close proximity of the six C−C bonds making up the very compact tetrahedrane cage **4** leads to the appearance of sizable-connected strongly shielded regions over these bonds. (The respective contour plot in Figure 3 shows that each of these regions bends out of the cage and that shielding decreases toward the cage center.)

The contour plots shown in Figure 3 provide more detailed information about the spatial variations in the isotropic shielding around **1**−**5**. Whereas the shielding contours outline the C−C bonds in **2**−**5** reasonably well, it turns out not to be at all straightforward to think of a way of separating the strongly shielded central region in **1** into contributions associated with individual bonds. On the other hand, there is not even a trace of a shielded central region in **3**. Indeed, the contour plots in the σ_h and σ_v symmetry planes of **3** show that shielding near the center of this molecule goes down to under 10 ppm. We note that the σ_h contour plot for **5** lends further support to the bent C−C bonds model of this molecule. Different extents of C−C bond outward "bending" are also observed in **2**, **3**, and **4**, but not in **1**. As can be seen from the contour plots obtained at the CASSCF(2,2) level, the size of the strongly shielded central region in **1** turns out to be larger at this level, in spite of the longer distance between the bridgehead carbon atoms; increased shielding is also observed within the three-membered ring in the CCC plane in **2**.

The methylene carbon atoms in **1** are surrounded by small ovoid deshielded regions inside which $\sigma_{iso}(\mathbf{r})$ becomes negative. (These regions are more obvious in the contour plots in Figure 3 and are more pronounced at the B3LYP level). Similar deshielded "halos" around sp^2 and sp hybridized carbon atoms and other sp^2 hybridized first main row atoms

https://doi.org/10.1021/acs.jpca.2c06450
J. Phys. Chem. A XXXX, XXX, XXX−XXX

have been observed previously in conjugated rings,[21,22,38,39] as well as in open-chain and conjugated molecules such as ethene, ethyne, and *s-trans*-1,3-butadiene.[18,19] These "halos" have been attributed to a specific type of π electron behavior that is a characteristic of some sp^2 and sp hybridized first main row atoms and that is different from traditional ring currents.[21] The occurrence of such "halos" around the methylene carbon atoms in **1** suggests a hybridization state that is in-between sp^2 and sp^3. There are no such "halos" around the bridgehead carbon atoms in **1** and **2**, or any of the carbon atoms in **4** and **5**; accordingly, the hybridization states of all of these carbon atoms are expected to be close to sp^3. The surroundings of the methylene carbon atoms in **2** and of all the carbon atoms in **3** do show some deshielding, less pronounced than that around the methylene carbon atoms in **1**, but still clearly noticeable, even in Figure 2 (see the almost spherical parts of the isotropic shielding isosurface at 16 ppm surrounding all carbon atoms in **3**). This does come as a surprise and while one interpretation could be that the carbon atoms in **3** also have hybridization states intermediate between sp^2 and sp^3, some of this deshielding could also be due to the longer wing C−C bonds. Very close to carbon nuclei, the isotropic shielding is always positive and it increases sharply, as has been shown in detail for the sp hybridized carbon atoms in C_2H_2.[19]

One notable feature of the isotropic shielding variations around **1** is the absence of shielded regions close to the bridgehead carbon atoms that would be expected to arise from "exo" sp^3-like HAOs on these atoms pointing outward of the [1.1.1]propellane cage. While at the B3LYP level, this could be partially attributed to the use of doubly occupied Kohn−Sham orbitals, the analogous CASSCF(2,2) isotropic shielding results indicate that this is indeed a feature of the shielding distribution in this molecule: We observe no increased shielding resulting from the two outward-directed orthogonal localized active space CASSCF(2,2) orbitals reported by Duarte and co-workers,[6] the shapes of which closely resemble "exo" sp^3-like HAOs. Moreover, the shielding picture around the bridgehead carbon atoms in **1** is markedly different from that for C_2, in which there are sizable regions of increased shielding outward of the C−C bond that are consistent with the shielding actions of two "exo" sp HAOs.[19] The shielding variations around **1** strongly suggest that the shielding activities of any HAOs on the bridgehead carbon atoms which are not involved in the C_b−C_m bonds are almost entirely contained within the [1.1.1]propellane cage.

The shielding picture outside the [1.1.1]propellane cage is consistent with the total electron density distribution in that region of space. The B3LYP and CASSCF(2,2) total electron density (ρ) contour plots shown in Figure 4 are reasonably similar. A notable feature of both of these plots is the lower electron density inside the [1.1.1]propellane cage, along the C_b−C_b direction, when compared to that along the C_b−C_m bonds. This is in agreement with the experimental and B3LYP/6-311G* static deformation densities for **1**.[40] While highlighting clearly the C_b−C_m bonds, the Laplacian of the total electron density ($\nabla^2\rho$), at either level of theory used here, does not show a C_b−C_b interaction of the same type (see Figure 4).

One argument that has often been used in support of the existence of a C_b−C_b bond is associated with the presence of a bond critical point (bcp) at the midpoint of the line connecting the two bridgehead carbon atoms.[40,41] However, while at the Hartree−Fock level (HF/6-31G*), the Laplacian at this bcp was found to be negative (−0.109 a.u.),[41] which is

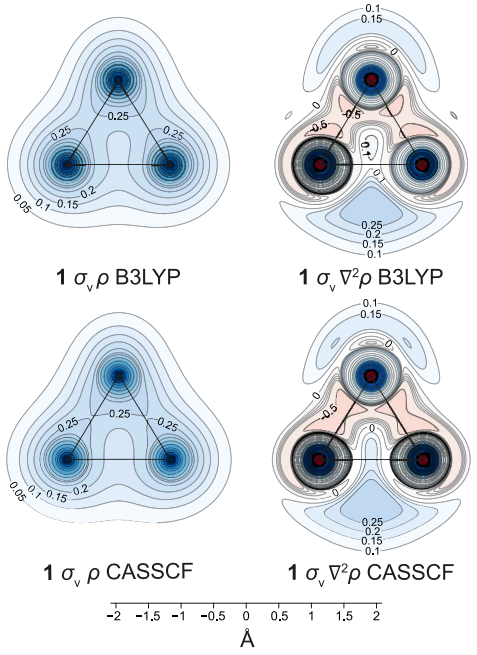

Figure 4. Total electron density (ρ) and Laplacian of the total electron density ($\nabla^2\rho$) contour plots in the σ_v symmetry plane of **1**, from calculations at the B3LYP/6-311++G(d,p)//B3LYP-D3(BJ)/def2-TZVP and CASSCF(2,2)/6-311++G(d,p)//CASSCF(2,2)/def2-TZVP levels. Lines show bonds in the plotting plane. ρ range between 0 and 75 a.u. (ρ, blue), $\nabla^2\rho$ range between ca. -10^5 and 300 a.u. ($\nabla^2\rho$, red to blue).

suggestive of some covalent bond character, subsequent evaluations[40] at the B3LYP/6-311G* level, and from experimental electron densities produced positive $\nabla^2\rho$ values of 0.083 and 0.427 a.u., respectively, which are more in line with a noncovalent interaction. Similarly, our B3LYP and CASSCF(2,2) values of $\nabla^2\rho$ at the midpoint of the C_b−C_b line, extracted from the data used to construct Figure 4, are 0.093 and 0.179 a.u., respectively, again suggestive of a noncovalent interaction. While still smaller than the experimental $\nabla^2\rho$ value, the CASSCF(2,2) result is a significant improvement, in the right direction, over that obtained at the B3LYP level.

It is important to note that the ρ and $\nabla^2\rho$ contour plots in Figure 4 do not display features that could be used to account for the presence of a strongly shielded region within the interior of the [1.1.1]propellane cage (see Figures 2 and 3). Still, by analogy to the increased shielding over chemical bonds observed in other molecules, it is logical to assume that this shielded region is linked to the existence of some form of bonding interaction. The appearance of this shielded region can be associated, in part, with the overlaps of the shielded regions over the six closely spaced C_b−C_m bonds and, indeed, the contour plots in Figure 3 show that the overlaps of the shielded regions over neighboring C−C bonds do increase in the sequence cyclopropane **5** (one three-membered carbon ring), bicyclo[1.1.0]butane **2** (two fused three-membered carbon rings), [1.1.1]propellane **1** (three three-membered carbon rings fused over the link between the bridgehead carbon atoms). On the other hand, such overlaps should be more pronounced in the even smaller interior of tetrahedrane **4** and yet the shielding decreases toward the center of the cage.

Further insights into the nature of the strongly shielded central region in **1** can be obtained by examining the

https://doi.org/10.1021/acs.jpca.2c06450
J. Phys. Chem. A XXXX, XXX, XXX−XXX

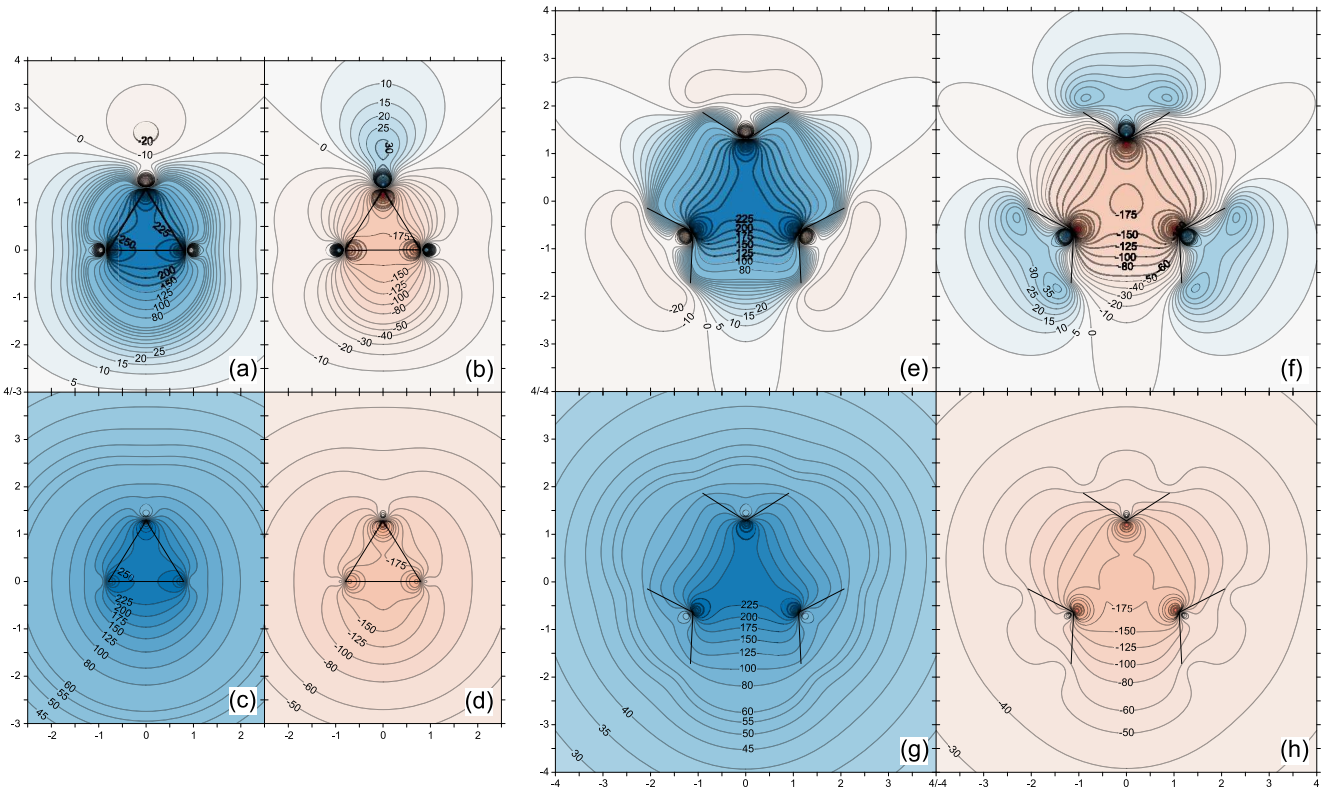

Figure 5. Contour plots of the diamagnetic (a, c, e, g) and paramagnetic (b, d, f, h) contributions to the isotropic shielding in **1** in the σ_v (a−d) and σ_h (e−h) symmetry planes from calculations at the CASSCF(2,2)-GIAO/6-311++G(d,p)//CASSCF(2,2)/def2-TZVP level. (a, b, e, f) were calculated with gauge origin at the center of mass; (c, d, g, h) were calculated with individual gauge origins at **r** for each $\boldsymbol{\sigma}(\mathbf{r})$. Lines show bonds in the plotting plane. The $\sigma^{d}_{iso}(\mathbf{r})$ and $\sigma^{p}_{iso}(\mathbf{r})$ ranges are between ca. −600 and 600 ppm, red/orange (deshielded) to blue (shielded), axes in Å.

diamagnetic and paramagnetic contributions to the off-nucleus isotropic shielding. As the CASSCF(2,2) level provides a more reliable picture of the electronic structure of **1**, the data for the $\sigma^{d}_{iso}(\mathbf{r})$ and $\sigma^{p}_{iso}(\mathbf{r})$ contour plots in Figure 5 come from calculations at this level rather than B3LYP. The diamagnetic and paramagnetic contributions depend on the choice of the gauge origin and there are two possible choices which ensure that these contributions reflect the full symmetry of **1**. The first of these is to go along with the standard single gauge origin at the center of mass, and the alternative is to use an individual gauge origin at **r** for each $\boldsymbol{\sigma}(\mathbf{r})$. We have carried out $\sigma^{d}_{iso}(\mathbf{r})$ and $\sigma^{p}_{iso}(\mathbf{r})$ calculations with each of these choices. In both cases, the calculations were performed using the natural connection.

As can be seen in Figure 5, the behavior of each of the diamagnetic and paramagnetic contributions inside the [1.1.1]propellane cage does not change much on switching from a single gauge origin at the center of mass to individual gauge origins at **r** for each $\boldsymbol{\sigma}(\mathbf{r})$: for either choice, $\sigma^{d}_{iso}(\mathbf{r})$ and $\sigma^{p}_{iso}(\mathbf{r})$ shield and deshield the interior of the cage, respectively. More pronounced differences are observed outside the [1.1.1]propellane cage: With a single gauge origin at the center of mass, $\sigma^{d}_{iso}(\mathbf{r})$ and $\sigma^{p}_{iso}(\mathbf{r})$ shield and deshield, respectively, the immediate surroundings of the cage, change sign in certain regions of space outside the cage, and the magnitudes of both contributions decrease quickly with increasing distance from the center of the cage. On the other hand, with individual gauge origins at **r** for each $\boldsymbol{\sigma}(\mathbf{r})$, $\sigma^{d}_{iso}(\mathbf{r})$ and $\sigma^{p}_{iso}(\mathbf{r})$ turn out to be uniformly positive and negative, respectively, and the magnitude of each of these contributions decreases slower with increasing distance from the center of the cage.

Interestingly, for either choice of gauge origin, inside the cage, the variations in both the shielding from $\sigma^{d}_{iso}(\mathbf{r})$ and the deshielding from $\sigma^{p}_{iso}(\mathbf{r})$ suggest that these could arise through the interactions between three Walsh-model-like sp^2 HAOs on the methylene carbon atoms, pointing toward the center of the cage and two sp^3 HAOs on the bridgehead carbon atoms. Of course, when added together, the $\sigma^{d}_{iso}(\mathbf{r})$ and $\sigma^{p}_{iso}(\mathbf{r})$ contour plots for either choice of gauge origin in Figure 5 reproduce the corresponding $\sigma_{iso}(\mathbf{r})$ contour plots in Figure 3, with shielding prevailing almost everywhere, but the details that can be associated with HAOs are no longer obvious. Similarly to the $\sigma_{iso}(\mathbf{r})$ contour plots in the σ_v plane (Figure 3), the corresponding $\sigma^{d}_{iso}(\mathbf{r})$ and $\sigma^{p}_{iso}(\mathbf{r})$ contour plots do not show significant shielding or deshielding outside the cage that could result from the two outward-directed orthogonal localized active space CASSCF(2,2) orbitals on the bridgehead carbon atoms. The observation that the diamagnetic contribution to the isotropic shielding, which depends on the electron density, behaves differently from the total electron density (compare the σ_v contour plots in Figures 4 and 5) lends further support to the argument that the shielding picture inside the [1.1.1]propellane cage would be very difficult to explain by examining only the total electron density and/or its Laplacian. The bonding interaction associated with the increased shielding within the [1.1.1]propellane cage can be overlooked by approaches that partition the total electron density into contributions from orbitals and/or VB structures, or that examine its Laplacian. Overall, our conclusion is that the shielding picture inside the [1.1.1]propellane cage suggests the existence of a bonding interaction which cannot be separated, in a straightforward fashion, into contributions from individual

https://doi.org/10.1021/acs.jpca.2c06450
J. Phys. Chem. A XXXX, XXX, XXX−XXX

carbon−carbon bonds. The bridgehead carbon atoms are fully engaged in this bonding interaction and, as mentioned above, the shielding activity of the "exo" sp^3-like HAOs is almost entirely contained within the cage.

While the accurate reproduction of the experimentally measured isotropic shieldings and chemical shifts in **1**−**5** is not amongst the aims of this paper, it is interesting to examine the extent to which our B3LYP-GIAO and CASSCF-GIAO results obtained using the 6-311++G(d,p) basis set (see Table 1) agree with experimental data and with other theoretical estimates. A detailed comparison between a number of theoretical estimates and experimental measurements of the isotropic shieldings of the nuclei in **1** and **3** has been carried out by Pecul and co-workers.[42] Despite the use of a slightly different geometry, our CASSCF(2,2) $\sigma_{iso}(^{13}C_b, \mathbf{1})$ value of 200.6 ppm is very close to their RAS-II/IGLO-III (restricted active space SCF with GIAOs) value of 199.2 ppm which, in turn, is in excellent agreement with the experiment. There is a larger difference between the CASSCF(2,2) and RAS-II/IGLO-III $\sigma_{iso}(^{13}C_m, \mathbf{1})$ values of 129.0 and 122.1 ppm, respectively; this can be attributed to the much smaller active space in the CASSCF(2,2) wavefunction, which is limited to just two orbitals on the bridgehead carbon atoms. Similar considerations apply to the difference between the CASSCF(2,2) and RAS-II/IGLO-III $\sigma_{iso}(^{1}H_m, \mathbf{1})$ values of 30.9 and 30.1 ppm. The B3LYP-GIAO $\sigma_{iso}(^{13}C)$ values for **1** obtained using the IGLO-III basis (177.9/100.0 ppm)[42] turned out to be lower than the experimental measurements. Our B3LYP $\sigma_{iso}(^{13}C)$ values are higher but still below the experimental values; B3LYP performs reasonably well for $\sigma_{iso}(^{1}H_m)$ in **1**. Additionally, some of the differences between our gas-phase CASSCF(2,2)-GIAO $\sigma_{iso}(^{13}C)$ values for **1** and **2**, and B3LYP-GIAO $\sigma_{iso}(^{13}C)$ values for **1**, **2**, and **5** are very close to the differences between the corresponding liquid NMR shielding constants, taken with negative signs.[43] CASSCF(2,2)-GIAO and B3LYP-GIAO calculations estimate the $\sigma_{iso}(^{13}C_b, \mathbf{1})-\sigma_{iso}(^{13}C_m, \mathbf{1})$ difference as 71.6 and 73.5 ppm, respectively (see Table 1), with the latter being very close to the liquid NMR value of 73.2 ppm; the CASSCF(2,2)-GIAO value is less accurate because of the small active space. Our CASSCF(2,2)-GIAO and B3LYP-GIAO $\sigma_{iso}(^{13}C_b, \mathbf{2})-\sigma_{iso}(^{13}C_b, \mathbf{1})$ differences are 2.9 and 3.0 ppm, respectively, against a liquid NMR difference of 4 ppm, and the CASSCF(2,2)-GIAO and B3LYP-GIAO $\sigma_{iso}(^{13}C_m, \mathbf{2})-\sigma_{iso}(^{13}C_m, \mathbf{1})$ differences are 40.5 and 43.3 ppm, respectively, against a liquid NMR difference of 41.2 ppm. At the B3LYP-GIAO level, $\sigma_{iso}(^{13}C_b, \mathbf{1})-\sigma_{iso}(^{13}C, \mathbf{5}) = -3.4$ ppm (from Table 1) is in excellent agreement with the liquid NMR difference of −3.8 ppm. All in all, as is to be expected from the literature,[44] shieldings calculated at the B3LYP-GIAO/6-311++G(d,p) level correlate well with experimental NMR data for molecules such as those included in Table 1, and it turns out that the CASSCF(2,2)-GIAO/6−311++G(d,p) level also performs reasonably well.

Table 1. Isotropic Shieldings of All Nuclei in [1.1.1]Propellane 1, Bicyclo[1.1.0]butane 2, Bicyclo[1.1.1]pentane 3, Tetrahedrane 4, Cyclopropane 5, Ethane, and Ethene (in ppm)[a]

molecule	method	$\sigma_{iso}(^{13}C)$	$\sigma_{iso}(^{1}H)$
1	B3LYP	183.1/109.6	30.3
	CASSCF	200.6/129.0	30.9
2	B3LYP	186.1/152.9	30.8/31.6/30.7
	CASSCF	203.5/169.5	31.2/32.1/31.3
3	B3LYP	147.5/131.0	29.5/30.2
4	B3LYP	211.8	29.1
5	B3LYP	186.5	32.1
ethane	B3LYP	176.3	31.2
ethene	B3LYP	53.8	26.3

[a]Gas-phase B3LYP-GIAO and CASSCF(2,2)-GIAO calculations in the 6-311++G(d,p) basis set at optimized or experimental geometries (for details, see text). $^{13}C_b/^{13}C_m$ values for **1**−**3**, $^{1}H_b/^{1}H_m$(axial)/$^{1}H_m$(equatorial) values for **2**, $^{1}H_b/^{1}H_m$ values for **3**.

Looking again at the B3LYP-GIAO results in Table 1, we observe that the $\sigma_{iso}(^{13}C_b, \mathbf{1})$ and $\sigma_{iso}(^{13}C, \mathbf{5})$ values are close to, but higher than, the carbon isotropic shielding in ethane, a molecule with sp^3 hybridized carbon atoms. This strengthens the argument made on the basis of the isotropic shielding plots for **1** and **5** (see Figure 3) that the hybridization states of the bridgehead carbon atoms in **1** and all of the carbon atoms in **5** should be close to sp^3. On the other hand, the $\sigma_{iso}(^{13}C_m, \mathbf{1})$ value lies between the carbon isotropic shieldings in ethane and ethene, but it is closer to that in ethene, consistent with the observation of the deshielded "halos" around the methylene carbon atoms in **1** (see Figure 3). The $\sigma_{iso}(^{13}C_b, \mathbf{2})$ and $\sigma_{iso}(^{13}C_m, \mathbf{2})$ values also lie between the carbon isotropic shieldings in ethane and ethene, but they are closer to that in ethane, consistent with the less pronounced deshielded "halos" around the respective carbon atoms that are observed in Figure 3.

The proton isotropic shieldings in **1** are higher than those in ethene and the $\sigma_{iso}(^{1}H_m)$ values decrease with the additions of the second and third fused three-membered rings in the sequence **5**, **2**, **1**. Even so, the $\sigma_{iso}(^{1}H_m)$ values in **1** and **2** remain closer to the proton isotropic shielding in ethane than to that in ethene. This is most likely due to the absence of π electron systems in **1** and **2** and should not be interpreted as an indication that the hybridization states of the methylene carbon atoms in these molecules are closer to sp^3 than to sp^2.

CONCLUSIONS

The off-nucleus isotropic magnetic shielding and its diamagnetic and paramagnetic contributions studied as functions of position in the space surrounding [1.1.1]-propellane show that the shielding activity of the two "exo" sp^3-like HAOs on the bridgehead carbon atoms (say, in the form of localized CASSCF orbitals) used to support the idea of an inverted bond between these carbons is almost entirely contained within the [1.1.1]propellane cage. We observe a strongly shielded central region within this cage that encloses most of its interior and extends over the middle parts of the wing C−C bonds. The diamagnetic and paramagnetic contributions to shielding within this region could be thought to arise through the interactions between three Walsh-model-like sp^2 HAOs on the methylene carbon atoms, pointing toward the center of the cage and two sp^3 HAOs on the bridgehead carbon atoms. The size and intensity of the central shielded region suggest the existence of a reasonably strong bonding interaction which cannot be separated, in a straightforward fashion, into contributions from individual carbon−carbon bonds; the bridgehead carbon atoms are fully engaged in this bonding interaction. Outside the cage, our results show no significant shielding next to the bridgehead carbon atoms. The comparison of the results of B3LYP and CASSCF(2,2) calculations on [1.1.1]propellane to those for

https://doi.org/10.1021/acs.jpca.2c06450
J. Phys. Chem. A XXXX, XXX, XXX−XXX

other molecules involving three-membered carbon rings, namely, bicyclo[1.1.0]butane, bicyclo[1.1.1]pentane, tetrahedrane, and cyclopropane, suggests that this interaction inside the [1.1.1]propellane cage is predominantly covalent in nature.

Of course, the electronic structure of [1.1.1]propellane could be interpreted in more than one way, for example, using localized MOs or different VB approaches, placing more or less emphasis on orbital shapes, overlaps, and ionic structures. A discussion of the pros and cons of such alternative interpretations of [1.1.1]propellane might not seem so dissimilar to comparisons between the alternative σ-π and bent-bond descriptions of multiple carbon−carbon bonds.[45−47] However, the magnetic shielding interpretation of bonding in this molecule would not change as it does not require the use of a specific wavefunction—as we have demonstrated, the analyses of B3LYP and CASSCF(2,2) isotropic shielding contour plots lead to essentially the same conclusions.

Our analysis of the off-nucleus isotropic magnetic shielding results for [1.1.1]propellane does of course challenge simple notions that the bonding in almost any molecule can be described by drawing lines connecting atoms—according to our results, the bonding interactions in tight spaces, such as in the [1.1.1]propellane cage, can be rather more complicated.

■ ASSOCIATED CONTENT

Supporting Information

The Supporting Information is available free of charge at https://pubs.acs.org/doi/10.1021/acs.jpca.2c06450.

Additional computational details and optimized geometries for [1.1.1]propellane, bicyclo[1.1.0]butane, bicyclo[1.1.1]pentane, and tetrahedrane (PDF)

Gaussian cube files with isotropic shielding values for [1.1.1]propellane, bicyclo[1.1.0]butane, bicyclo[1.1.1]-pentane, tetrahedrane, and cyclopropane (ZIP).

High resolution versions of all figures (ZIP)

■ AUTHOR INFORMATION

Corresponding Author

Peter B. Karadakov − *Department of Chemistry, University of York, York YO10 5DD, U.K.;* orcid.org/0000-0002-2673-6804; Email: peter.karadakov@york.ac.uk

Authors

Ben Stewart − *Department of Chemistry, University of York, York YO10 5DD, U.K.*

David L. Cooper − *Department of Chemistry, University of Liverpool, Liverpool L69 7ZD, U.K.;* orcid.org/0000-0003-0639-0794

Complete contact information is available at: https://pubs.acs.org/10.1021/acs.jpca.2c06450

Notes

The authors declare no competing financial interest.

■ ACKNOWLEDGMENTS

The authors thank the U.K. Engineering and Physical Sciences Research Council (EPSRC) for a Vacation Internship (EP/T518025/1) on behalf of B.S.

■ REFERENCES

(1) Levin, M. D.; Kaszynski, P.; Michl, J. Bicyclo[1.1.1]pentanes, [*n*]Staffanes, [1.1.1]Propellanes, and Tricyclo[2.1.0.0^{2,5}]pentanes. *Chem. Rev.* **2000**, *100*, 169−234.

(2) Wu, W.; Gu, J.; Song, J.; Shaik, S.; Hiberty, P. C. The Inverted Bond in [1.1.1]Propellane is a Charge-Shift Bond. *Angew. Chem., Int. Ed.* **2009**, *48*, 1407−1410.

(3) Shaik, S.; Danovich, D.; Galbraith, J. M.; Braïda, B.; Wu, W.; Hiberty, P. C. Charge-Shift Bonding: A New and Unique Form of Bonding. *Angew. Chem., Int. Ed.* **2020**, *59*, 984−1001.

(4) Laplaza, R.; Contreras-Garcia, J.; Fuster, F.; Volatron, F.; Chaquin, P. The "Inverted Bonds" Revisited: Analysis of "In Silico" Models and of [1.1.1]Propellane by Using Orbital Forces. *Chem. − Eur. J.* **2020**, *26*, 6839−6845.

(5) Braïda, B.; Shaik, S.; Wu, W.; Hiberty, P. C. Comment on "The 'Inverted Bonds' Revisited. Analysis of 'in Silico' Models and of [1.1.1]Propellane Using Orbital Forces". *Chem. − Eur. J.* **2020**, *26*, 6935−6939.

(6) Sterling, A. J.; Dürr, A. B.; Smith, R. C.; Anderson, E. A.; Duarte, F. Rationalizing the diverse reactivity of [1.1.1]propellane through σ−π-delocalization. *Chem. Sci.* **2020**, *11*, 4895−4903.

(7) Feller, D.; Davidson, E. R. Ab initio studies of [1.1.1]- and [2.2.2]propellane. *J. Am. Chem. Soc.* **1987**, *109*, 4133−4139.

(8) Chen, Z.; Wannere, C. S.; Corminboeuf, C.; Puchta, R.; Schleyer, P. v. R. Nucleus-Independent Chemical Shifts (NICS) as an Aromaticity Criterion. *Chem. Rev.* **2005**, *105*, 3842−3888.

(9) Schleyer, P. v. R.; Maerker, C.; Dransfeld, A.; Jiao, H.; van Eikema Hommes, N. J. R. Nucleus-Independent Chemical Shifts: A Simple and Efficient Aromaticity Probe. *J. Am. Chem. Soc.* **1996**, *118*, 6317−6318.

(10) Wolinski, K. Magnetic shielding surface in molecules. Neutron as a probe in the hypothetical magnetic resonance spectroscopy. *J. Chem. Phys.* **1997**, *106*, 6061−6067.

(11) Klod, S.; Kleinpeter, E. J. Ab initio calculation of the anisotropy effect of multiple bonds and the ring current effect of arenes—application in conformational and configurational analysis. *J. Chem. Soc., Perkin Trans. 2* **2001**, 1893−1898.

(12) Gauss, J. Effects of electron correlation in the calculation of nuclear magnetic resonance chemical shifts. *J. Chem. Phys.* **1993**, *99*, 3629−3643.

(13) Gauss, J.; Stanton, J. F. Coupled-cluster calculations of nuclear magnetic resonance chemical shifts. *J. Chem. Phys.* **1995**, *103*, 3561−3577.

(14) Ruud, K.; Helgaker, T.; Bak, K. L.; Jørgensen, P.; Olsen, J. Accurate magnetizabilities of the isoelectronic series BeH^-, BH, and CH^+. The MCSCF-GIAO approach. *Chem. Phys.* **1995**, *195*, 157−169.

(15) Olsen, J.; Bak, K. L.; Ruud, K.; Helgaker, T.; Jørgensen, P. Orbital connections for perturbation-dependent basis sets. *Theor. Chim. Acta* **1995**, *90*, 421−439.

(16) Ruud, K.; Helgaker, T.; Olsen, J.; Jørgensen, P.; Bak, K. L. A numerically stable orbital connection for the calculation of analytical Hessians using perturbation-dependent basis sets. *Chem. Phys. Lett.* **1995**, *235*, 47−52.

(17) Iliaš, M.; Jensen, H. J. A.; Bast, R.; Saue, T. Gauge origin independent calculations of molecular magnetisabilities in relativistic four-component theory. *Mol. Phys.* **2013**, *111*, 1373−1381.

(18) Karadakov, P. B.; Horner, K. E. Exploring Chemical Bonds through Variations in Magnetic Shielding. *J. Chem. Theory Comput.* **2016**, *12*, 558−563.

(19) Karadakov, P. B.; Kirsopp, J. Magnetic Shielding Studies of C_2 and C_2H_2 Support Higher than Triple Bond Multiplicity in C_2. *Chem. − Eur. J.* **2017**, *23*, 12949−12954.

(20) Jackson, J. E.; Allen, L. C. The C_1−C_3 Bond in [1.1.1]-Propellane. *J. Am. Chem. Soc.* **1984**, *106*, 591−599.

(21) Karadakov, P. B.; Horner, K. E. Magnetic Shielding in and around Benzene and Cyclobutadiene: A Source of Information about Aromaticity, Antiaromaticity, and Chemical Bonding. *J. Phys. Chem. A* **2013**, *117*, 518−523.

(22) Karadakov, P. B.; Hearnshaw, P.; Horner, K. E. Magnetic Shielding, Aromaticity, Antiaromaticity, and Bonding in the Low-Lying Electronic States of Benzene and Cyclobutadiene. *J. Org. Chem.* **2016**, *81*, 11346−11352.
(23) Karadakov, P. B.; Preston, N. Aromaticity reversals and their effect on bonding in the low-lying electronic states of cyclooctatetraene. *Phys. Chem. Chem. Phys.* **2021**, *23*, 24750−24756.
(24) Frisch, M. J.; Trucks, G. W.; Schlegel, H. B.; Scuseria, G. E.; Robb, M. A.; Cheeseman, J. R.; Scalmani, G.; Barone, V.; Petersson, G. A.; Nakatsuji, H.; et al.*Gaussian 16, Revision A.03*; Gaussian, Inc.: Wallingford CT, 2016.
(25) Endo, Y.; Chang, M. C.; Hirota, E. The microwave spectrum of cyclopropane-1,1-d_2 molecular structure of cyclopropane. *J. Mol. Spectrosc.* **1987**, *126*, 63−71.
(26) See https://gaussian.com/cubegen/ (accessed Oct 30, 2022).
(27) Duncan, J. L.; McKean, D. C.; Bruce, A. J. Infrared spectroscopic studies of partially deuterated ethanes and the r_0, r_z, and r_e structures. *J. Mol. Spectrosc.* **1979**, *74*, 361−374.
(28) Harmony, M. D. The equilibrium carbon−carbon single-bond length in ethane. *J. Chem. Phys.* **1990**, *93*, 7522−7523.
(29) Craig, N. C.; Groner, P.; McKean, D. C. Equilibrium Structures for Butadiene and Ethylene: Compelling Evidence for Π-Electron Delocalization in Butadiene. *J. Phys. Chem. A* **2006**, *110*, 7461−7469.
(30) Aidas, K.; Angeli, C.; Bak, K. L.; Bakken, V.; Bast, R.; Boman, L.; Christiansen, O.; Cimiraglia, R.; Coriani, S.; Dahle, P.; et al. The Dalton quantum chemistry program system. *Wiley Interdiscip. Rev.: Comput. Mol. Sci.* **2014**, *4*, 269−284. Dalton, a Molecular Electronic Structure Program, Release Dalton2020.1, 2022. http://daltonprogram.org (accessed Oct 30, 2022).
(31) Hedberg, L.; Hedberg, K. The molecular structure of gaseous [1.1.1]propellane: an electron-diffraction investigation. *J. Am. Chem. Soc.* **1985**, *107*, 7257−7260.
(32) Almenningen, A.; Andersen, B.; Nyhus, B. A.; Beronius, P.; Engebretsen, J. E.; Ehrenberg, L. On the Molecular Structure of Bicyclo(1.1.1)pentane in the Vapour Phase Determined by Electron Diffraction. *Acta Chem. Scand.* **1971**, *25*, 1217−1223.
(33) Cox, K. W.; Harmony, M. D.; Nelson, G.; Wiberg, K. B. Microwave Spectrum and Structure of Bicyclo[1.1.0]butane. *J. Chem. Phys.* **1969**, *50*, 1976−1980.
(34) Perry, A.; Martin, M. A.; Nibler, J. W.; Maki, A.; Weber, A.; Blake, T. A. Coriolis analysis of several high-resolution infrared bands of bicyclo[111]pentane-d_0 and -d. *J. Mol. Spectrosc.* **2012**, *276*−*277*, 22−32.
(35) Coulson, C. A.; Moffitt, W. E. I. The properties of certain strained hydrocarbons. *Philos. Mag.* **1949**, *40*, 1−35.
(36) Karadakov, P. B.; Gerratt, J.; Cooper, D. L.; Raimondi, M. The Nature of the Carbon-Carbon Bonds in Cyclopropane and Cyclobutane: A Comparison Based on Spin-Coupled Theory. *J. Am. Chem. Soc.* **1994**, *116*, 7714−7721.
(37) Walsh, A. D. The structures of ethylene oxide, cyclopropane, and related molecules. *Trans. Faraday Soc.* **1949**, *45*, 179−190.
(38) Horner, K. E.; Karadakov, P. B. Chemical Bonding and Aromaticity in Furan, Pyrrole, and Thiophene: A Magnetic Shielding Study. *J. Org. Chem.* **2013**, *78*, 8037−8043.
(39) Horner, K. E.; Karadakov, P. B. Shielding in and around Oxazole, Imidazole, and Thiazole: How Does the Second Heteroatom Affect Aromaticity and Bonding? *J. Org. Chem.* **2015**, *80*, 7150−7157.
(40) Messerschmidt, M.; Scheins, S.; Grubert, L.; Pätzel, M.; Szeimies, G.; Paulmann, C.; Luger, P. Electron Density and Bonding at Inverted Carbon Atoms: An Experimental Study of a [1.1.1]-Propellane Derivative. *Angew. Chem., Int. Ed.* **2005**, *44*, 3925−3928.
(41) Wiberg, K. B.; Bader, R. F. W.; Lau, C. D. H. Theoretical analysis of hydrocarbon properties. 1. Bonds, structures, charge concentrations, and charge relaxations. *J. Am. Chem. Soc.* **1987**, *109*, 985−1001.
(42) Pecul, M.; Dodziuk, H.; Jaszuński, M.; Lukin, O.; Leszczyński, J. Ab initio calculations of the NMR spectra of [1.1.1]propellane and bicyclo[1.1.1]pentane. *Phys. Chem. Chem. Phys.* **2001**, *3*, 1986−1991.
(43) Orendt, A. M.; Facelli, J. C.; Grant, D. M.; Michl, J.; Walker, F. H.; Dailey, W. P.; Waddell, S. T.; Wiberg, K. B.; Schindler, M.; Kutzelnigg, W. Low temperature ^{13}C NMR magnetic resonance in solids 4. Cyclopropane, bicyclo[1.1.0]butane and [1.1.1] propellane. *Theor. Chim. Acta* **1985**, *68*, 421−430.
(44) Cheeseman, J. R.; Trucks, G. W.; Keith, T. A.; Frisch, M. J. A comparison of models for calculating nuclear magnetic resonance shielding tensors. *J. Chem. Phys.* **1996**, *104*, 5497−5509.
(45) Palke, W. E. Double bonds are bent equivalent hybrid (banana) bonds. *J. Am. Chem. Soc.* **1986**, *108*, 6543−6544.
(46) Karadakov, P. B.; Gerratt, J.; Cooper, D. L.; Raimondi, M. Bent versus σ-π bonds in ethene and ethyne: the spin-coupled point of view. *J. Am. Chem. Soc.* **1993**, *115*, 6863−6869.
(47) Ogliaro, F.; Cooper, D. L.; Karadakov, P. B. Bent-bond versus separated-bond models: A spin-coupled survey for a few organic and inorganic systems. *Int. J. Quantum Chem.* **1999**, *74*, 223−229.

https://doi.org/10.1021/acs.jpca.2c06450
J. Phys. Chem. A XXXX, XXX, XXX−XXX